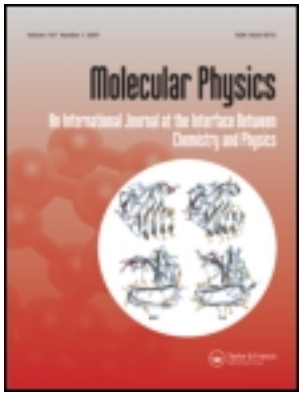

Molecular Physics: An International Journal at the Interface Between Chemistry and Physics

Publication details, including instructions for authors and subscription information:
http://www.tandfonline.com/loi/tmph20

Computer simulation of charged hard spherocylinders at low temperatures

Guadalupe Jiménez-Serratos [a] , Carlos Avendaño [b] , Alejandro Gil-Villegas [a] & Enrique González-Tovar [c]

[a] Departmento de Ingeniería Física, División de Ciencias e Ingenierías Campus León, Universidad de Guanajuato, Colonia Lomas del Campestre, León 37150, México

[b] Department of Chemical Engineering, Imperial College London, South Kensington Campus, London SW7 2AZ, UK

[c] Instituto de Física, Universidad Autónoma de San Luis Potosí, Álvaro Obregón 64, 78000 San Luis Potosí, S.L.P., México

Available online: 12 Nov 2010

To cite this article: Guadalupe Jiménez-Serratos, Carlos Avendaño, Alejandro Gil-Villegas & Enrique González-Tovar (2011): Computer simulation of charged hard spherocylinders at low temperatures, Molecular Physics: An International Journal at the Interface Between Chemistry and Physics, 109:1, 27-36

To link to this article: http://dx.doi.org/10.1080/00268976.2010.524171

Molecular Physics
Vol. 109, No. 1, 10 January 2011, 27–36

Taylor & Francis
Taylor & Francis Group

INVITED ARTICLE

Computer simulation of charged hard spherocylinders at low temperatures

Guadalupe Jiménez-Serratos[a], Carlos Avendaño[b], Alejandro Gil-Villegas[a]* and Enrique González-Tovar[c]

[a]*Departmento de Ingeniería Física, División de Ciencias e Ingenierías Campus León, Universidad de Guanajuato, Colonia Lomas del Campestre, León 37150, México;* [b]*Department of Chemical Engineering, Imperial College London, South Kensington Campus, London SW7 2AZ, UK;* [c]*Instituto de Física, Universidad Autónoma de San Luis Potosí, Álvaro Obregón 64, 78000 San Luis Potosí, S.L.P., México*

(*Received 12 August 2010; final version received 9 September 2010*)

In this work we report the stability of liquid crystalline phases of charged hard spherocylinders (CHSC) of aspect ratio $L/\sigma=5$ at low temperatures using NPT Monte Carlo computer simulations. Following the methodology used in previous work [C. Avendaño, A. Gil-Villegas, E. González-Tovar, J. Chem. Phys. **128**, 044506 (2008); Chem. Phys. Lett. **470**, 67 (2009)], long-range coulombic interactions are handled using the Wolf method. The supramolecular organization of CHSC is obtained by compression of a low-density isotropic state. The system under consideration exhibits the expected isotropic, nematic, smectic-A, and crystal phases. However two important phenomena emerge at low temperatures, namely the existence of an isotropic–nematic–smectic triple point, with the ending of the nematic phase for lower temperatures, and the apparent hexatic arrangement of the layers in the smectic phases. Assuming that the smectic-layers behave as quasi-bidimensional systems, lowering the temperatures is possible to observe the formation of hexatic phases, which are detected analysing the structure factor, order parameters and distribution functions. This hexatic ordering indicates that the CHSC phase diagram presents a smectic-B phase at low temperatures.

Keywords: liquid crystals; computer simulation; Monte Carlo method

1. Introduction

Hard convex particles represent very simple models to describe liquid crystalline (LC) materials [1]. Since the pioneering work of Onsager it is well known that very long rods interacting only via a hard-core potential present an isotropic–nematic phase transition [2]. Such transition is a characteristic phenomenon displayed by real liquid crystals. For particles with finite aspect ratio, computer simulation is a powerful tool to provide exact results about the behaviour of the existing phases. In order to study systems of elongated molecules, one of the simplest geometries to consider is that of the spherocylinder, which is composed of a cylinder of length L capped at each end with a hemispherical part of diameter σ. Thus, the geometry of this model is fully characterized by the aspect ratio $L^*=L/\sigma$. This system of hard spherocylinders (HSC) has been investigated, for different values of L^*, by many authors [3–5]. In these works, the phase diagram of HSC has been characterized and the existence of isotropic (I), nematic (N), smectic-A (SmA) and crystalline (K) phases has been firmly established when $L^*\geq 4$. On the other hand, real LC molecules present different interactions, like charge–charge, dipole–dipole and $\pi-\pi$ interactions, in addition to short-range repulsive forces [6]. In this context, and looking for a more faithful model of substances that could exhibit orientational and positional order (e.g. ionic rodlike colloids, virus and other relevant biomaterials), recently, we have presented a computer simulation study of HSC interacting with a coulombic potential [7], i.e. of charged hard spherocylinders (CHSC). In [7] the phase diagram and the thermodynamic and structural properties of an electroneutral mixture of CHSC, with an aspect ratio of $L^*=5$, were investigated along two isotherms at a relative high temperature regime. Similarly for the cases of non-polar HSC and HSC with central longitudinal [8–10], central terminal [10–12], and central transverse point dipoles [10,13], the CHSC system presents

*Corresponding author. Email: gil@fisica.ugto.mx

ISSN 0026–8976 print/ISSN 1362–3028 online

DOI: 10.1080/00268976.2010.524171
http://www.informaworld.com

I, N, and SmA phases, although the ranges for which the CHSC phases appear are modified by the particular effect of the coulombic interaction. Interestingly, in the smectic configurations of CHSC a clear evidence of ion pairing was found. This ion pairing phenomenon is distinctive of charged systems (e.g. simple electrolytes) and its origin can be traced back to the electroneutrality condition assumed in this kind of system. One of the conclusions offered in [7] also pointed to the pertinence of a further study of CHSC at the low temperature region and the possible existence of an isotropic–nematic–smectic triple point.

Moreover, in a later work [14] we extended the investigation of coulombic rods by undertaking the analysis of a mixture of CHSC (with charges located at the centre or at the end of the spherocylinders) and charged hard spheres (CHS), as an attempt to model dispersions of electrified anisotropic molecules in the presence of their counterions. Therein, and apart from the recurrent ionic pairing phenomenon, a notable fact now raised in the case of CHSC with a charge placed at the centre, is the formation of columns of spherocylinders in hexagonal order in the planes perpendicular to the directors (i.e. an hexagonal columnar phase). This interesting event then poses the questions (a) are such phases exclusive of the mixture CHSC + CHS (i.e. if they are absent in systems of pure CHSC), and (b) is the hexagonal ordering in ionic LC induced by the Coulomb interaction and/or is the phenomenon detected by the fact of looking for the quasi-bidimensional (quasi-2D) planes in the smectic phases? It is worth mentioning that, to the best of our knowledge, an hexatic phase has not been observed yet in simulations or theories of charged or dipolar hard spherocylinders.

Motivated by the findings of these foregoing papers on CHSC, in the present communication we have proceeded to study a binary electroneutral mixture of CHSC at low temperatures, in order to perform a more exhaustive characterization of the phase diagram and of the associated thermodynamics and structural features, complementing the previous Monte Carlo investigation of [7].

2. Model and simulation details

The liquid crystalline behaviour of an electroneutral 1:1 charged hard spherocylinder (CHSC) system is studied using isobaric–isothermal Monte Carlo (NPT-MC) computer simulations. The interaction between a pair of particles, which contains both a hard body contribution and the coulombic term, is given by [15,16]

$$u_{ij} = u_{ij}^{\mathrm{hb}}(\boldsymbol{r}_{ij}, \omega_i, \omega_j) + \frac{q_i q_j}{D r_{ij}}, \tag{1}$$

where q_i is the charge of the particle i, D is the dielectric constant of the surrounding media, $\boldsymbol{r}_{ij}$ is the inter-particle vector between the centre of mass of particles i and j, $r_{ij} = |\boldsymbol{r}_{ij}|$, and ω_i denotes the orientation of the principal molecular axis of particle i. The term u_{ij}^{hb} in Equation (1) is the hard body contribution between a pair of hard spherocylinders represented as

$$u_{ij}^{\mathrm{hb}}(\boldsymbol{r}_{ij}, \omega_i, \omega_j) = \begin{cases} \infty, & \text{if} \quad \boldsymbol{r}_{ij} \in V_{\mathrm{ex}}(\omega_i, \omega_j), \\ 0, & \text{if} \quad \boldsymbol{r}_{ij} \notin V_{\mathrm{ex}}(\omega_i, \omega_j), \end{cases} \tag{2}$$

where V_{ex} is the excluded volume between two particles.

We introduce reduced units to describe the different thermodynamic states. Reduced temperature and pressure, as well as packing fraction, are defined as: $T^* = kTD\sigma/(z_+ z_- e^2)$, $P^* = P v_{\mathrm{p}}/(kT)$, and $\eta = N v_{\mathrm{p}}/V$, where k is the Boltzmann constant, T is the absolute temperature, σ is the diameter of the particles, z_i is the valence of species i, e is the protonic charge, N is the total number of particles, V is the volume of the system, P is the pressure, and $v_p = \pi\sigma^3/6 + \pi\sigma^2 L/4$ is the molecular volume of each particle.

The simulations are started using a face centred cubic lattice as an initial configuration [3,4,7]. It is possible to construct an almost cubic simulation box by carefully choosing the number of replicas of the unit cell in the three cartesian coordinates. In this work the simulation box was designed for a number of $N = 1020$ spherocylinders [4]. Once the initial lattice is constructed, NPT-MC simulations are performed at low pressures to obtain a low density isotropic state at a given temperature. Further compression of this initial isotropic state is done to obtain high density thermodynamic states within the isotherm.

As in our previous work [7,14,17,18] coulombic interactions are handled using the Wolf method [19,20], which has also been proved in other works by different authors to be in good agreement with MC predictions for homogeneous systems using the standard Ewald summation [21–24]. Although there has been some controversy in relation to the use of the Wolf method, this is related to the expression for the force in Molecular Dynamics studies [22–25], and not with the expression for the potential energy, which is the only requirement for MC studies.

The expression within the Wolf approach to account for the potential energy is a shifted and

damped potential that is given by the following expression:

$$U(R_c) = \frac{1}{2}\sum_{i=1}^{N}\sum_{\substack{j\neq i \\ (r_{ij}<R_c)}}\left(\frac{q_i q_j \mathrm{erfc}(\alpha r_{ij})}{r_{ij}} - \frac{q_i q_j \mathrm{erfc}(\alpha R_c)}{R_c}\right) - \left(\frac{\mathrm{erfc}(\alpha R_c)}{2R_c} + \frac{\alpha}{\pi^{1/2}}\sum_{i=1}^{N} q_i^2\right), \quad (3)$$

where R_c is the cut-off of the potential and α is a damping parameter that controls the range of the effective potential. The first term on the right-hand side of Equation (3) is the effective potential between a pair of particles and the second term is a self-consistent term. It has been shown in previous work that a single pair of R_c and α values are able to reproduce thermodynamic and structural properties of a broad number of charged systems ranging from simple spherical electrolytes to charged liquid crystals [7,14,17], when compared with the prediction made by the Ewald method [15,16,26–28]. The value of the Wolf parameters used are $R_c = 0.5\,\mathcal{L}_{\min}$ and $\alpha = 4.0/\mathcal{L}_{\min}$, where $\mathcal{L}_{\min}$ is the shortest simulation box length. A NPT MC cycle is defined as N trial displacements supplemented with a trial change on the system volume. In most of the simulations, between $1\times10^6 - 2\times10^6$ cycles are used to equilibrate the system and usually the same number of cycles to collect ensemble averages. Near to phase transitions, more cycles are required to obtain reliable results. The maximum allowed displacement, re-orientation and change of volume are adjusted to reach acceptable probabilities between 30–40%.

In order to detect the formation of mesophases, different order parameters and distribution functions may be used. The orientational order can be examined from the second-rank Saupe order tensor $\mathbf{Q}$, defined as [1,29]:

$$\mathbf{Q} = \frac{1}{N}\sum_{i=1}^{N}\left(\frac{3}{2}\hat{u}_i \otimes \hat{u}_i - \frac{\mathbf{I}}{2}\right), \quad (4)$$

where $\hat{\mathbf{u}}_i$ is a unit vector along the molecular axis of particle j, $\otimes$ indicates the dyadic product, and $\mathbf{I}$ is the second-rank unit tensor. Diagonalization of the tensor produces three eigenvalues and their respective eigenvectors. The nematic order parameter S is defined as the largest eigenvalue, and the corresponding eigenvector is often called the system director, $\boldsymbol{n}$. The order of the system can be monitored through the orientational correlation function $g_2(r)$, obtained as the average value of the second-order Legendres' polynomial for the angle between a pair of particles [30].

In order to detect the formation of smectic phases, the projection of the pair correlation function along the director, $g_{||}(r_{||})$, is evaluated. This correlation function provides information about the probability of finding a molecule in cylindrical shells along the director. The appearance of modulated peaks indicates the formation of layers that characterize smectic phases. The structure of the particles belonging to a given layer can be monitored using the related projection of the pair correlation function perpendicular to the director, $g_\perp(r_\perp)$, which may help to identify the arrangement of the particles in the plane of the layers. Direct visualization of the order in different planes of the system, specifically in the planes of the layers in smectic phases, can be obtained by means of the projection of the structure factor $S_\perp(\boldsymbol{q}_\perp)$ in the planes of the layers themselves [14,31,32]. This is similar to real scattering experiments, where different patterns depending on the structure are obtained. The structure factor is needed to recognize a possible transition between liquid-like structure, that characterizes smectic-A (SmA) phases, and hexatic-like structure, typically of smectic-B (SmB) phases. The structure factor is defined as

$$S_\perp(\boldsymbol{q}_\perp) = \frac{1}{N}\sum_n\sum_m \exp\left(\imath \boldsymbol{q}_\perp \cdot \boldsymbol{r}_{nm}\right), \quad (5)$$

where $\boldsymbol{q}_\perp$ is the projection of the wave number vector in the plane perpendicular to the director and $\boldsymbol{r}_{nm}$ is the interparticle vector position. In a similar way, the structure factors for different species, i.e. cation–cation and cation–anion, are also useful to identify the arrangement of the charges in the planes of the layers. Finally, to support the information obtained by the structure factor, we have calculated the hexagonal bond orientational parameter, Ψ_6, which is defined as:

$$\Psi_6 = \left\langle \frac{\left|\sum_{i=1}^{N-1}\sum_{j>i}^{N} p_{ij}\exp(\imath 6\theta_{ij})\right|}{\sum_{i=1}^{N-1}\sum_{j>i}^{N} p_{ij}} \right\rangle, \quad (6)$$

where θ_{ij} is the angle between the vector $\boldsymbol{r}_{ij}$ joining the centre of mass of the ith and jth molecules and a fixed axis perpendicular to the director. The pre-factor p_{ij}, simply restricts the summation only to the nearest neighbour particles for a given particle, and is defined in this work as

$$p_{ij} = \begin{cases} 1, & 1.10 <= r_{ij} <= 1.75, \\ 0, & \text{otherwise}, \end{cases} \quad (7)$$

where $r_{\perp ij}$ is the projection of the interparticle vector position in the plane perpendicular to the director. This parameter can take values in the range $0 \le \Psi_6 \le 1$, with $\Psi_6 = 1$ being the case where the particles have a

Table 1. NPT-MC simulation results for the pressure P^*, packing fraction η, order parameter S, excess internal energy U^{exc}/NkT and type of liquid crystalline phase. Results for a system of N=1020 charged hard spherocylinders with $L/\sigma = 5$ at a temperature of $T^* = 0.2$.

P^*	η	S	$-U^{exc}/NkT$	Phase
1.00	0.224 ± 0.002	0.032 ± 0.012	1.674 ± 0.021	I
2.00	0.292 ± 0.002	0.038 ± 0.010	1.840 ± 0.022	I
3.00	0.339 ± 0.002	0.049 ± 0.016	1.956 ± 0.022	I
4.00	0.377 ± 0.002	0.067 ± 0.020	2.059 ± 0.021	I
4.25	0.387 ± 0.002	0.091 ± 0.026	2.094 ± 0.024	I
4.50	0.395 ± 0.002	0.142 ± 0.037	2.108 ± 0.023	I
4.75	0.405 ± 0.002	0.152 ± 0.046	2.151 ± 0.026	I
5.00	0.414 ± 0.002	0.166 ± 0.034	2.176 ± 0.022	I
5.25	0.434 ± 0.002	0.641 ± 0.027	2.254 ± 0.025	N
5.50	0.480 ± 0.003	0.892 ± 0.005	2.542 ± 0.024	SmA
5.75	0.488 ± 0.003	0.899 ± 0.006	2.578 ± 0.025	SmA
6.00	0.495 ± 0.003	0.902 ± 0.005	2.609 ± 0.023	SmA
6.25	0.503 ± 0.002	0.912 ± 0.005	2.637 ± 0.025	SmA
6.50	0.510 ± 0.002	0.913 ± 0.006	2.659 ± 0.021	SmA
6.75	0.519 ± 0.003	0.922 ± 0.005	2.685 ± 0.022	SmA
7.00	0.523 ± 0.002	0.921 ± 0.006	2.694 ± 0.024	SmA
7.25	0.529 ± 0.002	0.923 ± 0.008	2.717 ± 0.023	SmA
7.50	0.536 ± 0.002	0.930 ± 0.005	2.725 ± 0.022	SmA
7.75	0.541 ± 0.003	0.929 ± 0.009	2.732 ± 0.020	SmA
8.00	0.544 ± 0.002	0.931 ± 0.008	2.743 ± 0.020	SmA
8.25	0.553 ± 0.002	0.939 ± 0.004	2.765 ± 0.021	SmA
8.50	0.555 ± 0.002	0.938 ± 0.005	2.766 ± 0.021	SmA
8.75	0.561 ± 0.002	0.942 ± 0.004	2.784 ± 0.019	SmA
9.00	0.566 ± 0.003	0.945 ± 0.003	2.795 ± 0.021	SmA
9.25	0.570 ± 0.002	0.947 ± 0.004	2.789 ± 0.022	SmA
9.50	0.573 ± 0.002	0.947 ± 0.004	2.801 ± 0.020	SmA
9.75	0.580 ± 0.003	0.950 ± 0.003	2.807 ± 0.023	SmA
10.00	0.584 ± 0.002	0.950 ± 0.004	2.818 ± 0.018	SmA
10.25	0.587 ± 0.002	0.951 ± 0.003	2.817 ± 0.021	SmA
10.40	0.589 ± 0.002	0.951 ± 0.004	2.830 ± 0.018	SmA
10.50	0.594 ± 0.003	0.954 ± 0.004	2.831 ± 0.019	SmB
10.60	0.595 ± 0.003	0.952 ± 0.004	2.840 ± 0.016	SmB
10.68	0.599 ± 0.002	0.956 ± 0.002	2.843 ± 0.018	SmB
10.75	0.616 ± 0.003	0.966 ± 0.001	2.789 ± 0.016	K
11.00	0.623 ± 0.003	0.967 ± 0.001	2.780 ± 0.014	K

perfect hexagonal arrangement and $\Psi_6 = 0$ in the absence of such an ordering.

3. Results

In Table 1, the results for the packing fraction, η, nematic order parameter, S, excess internal energy, U^{exc}/NkT, and type of LC phase are presented for the isotherm at $T^* = 0.2$. The behaviour of the pressure, P^*, as a function of the packing fraction, η, is shown in Figure 1. As a comparison, results for HSC [4], and for CHSC at temperature $T^* = 0.5$ [7] are also presented. Upon compression starting from a low-density I state, both an I–N and a N–SmA phase transition can be observed. The former phase transition going from an isotropic state ($\eta = 0.414$, $S = 0.166$) to a nematic state

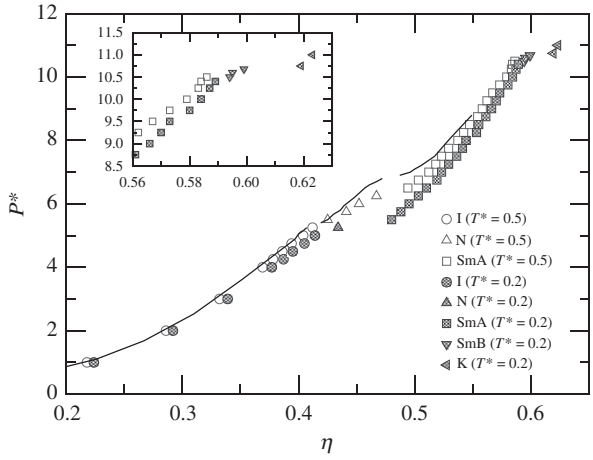

Figure 1. Pressure, P^*, as a function of the packing fraction for a system of 1020 CHSC of aspect ratio $L/\sigma = 5$ obtained by NPT-MC simulations. Open and shaded symbols correspond to temperatures $T^* = 0.5$ [7] and $T^* = 0.2$, respectively. The lines correspond to the HSC data reported by McGrother *et al.* [4].

($\eta = 0.434$, $S = 0.641$), and the latter going from a nematic state ($\eta = 0.434$, $S = 0.641$) to a smectic-A phase ($\eta = 0.480$, $S = 0.892$). Snapshots of the different LC phases observed at this temperature are presented in Figure 2. The I–N phase transition can be easily detected by means of the behaviour of the nematic order, which is shown in Figure 3. In this figure, a discontinuity of this parameter at the I–N phase transition can be observed. This discontinuity is characteristic of a first order phase transition. It is possible to obtain further information analysing the orientational correlation function, $g_2(r)$. This correlation function, depicted in Figure 4, has a fast decay to zero for isotropic phases, and a non-zero limit value at long distances for ordered phases. In the N phase, this limit value is proportional to S^2, i.e. $g_2(r \to \infty) \sim S^2$ [3]. As reported in our previous work for CHSC [7], the effect of the coulombic interactions is reflected in the systematic lowering of the coexistence pressure with respect to the non-coulombic case (see Figure 1). Moreover, it is also observed at low temperatures that the range of stability of the nematic phase also decreases compared with CHSC at high temperatures and with non-coulombic HSC. The effect of coulombic forces in CHSC is to enhance the range of stability of the isotropic phase compared with the non-coulombic HSC case. However, this enhancement is reduced as the temperature is decreased. This pattern has also been observed in dipolar LC systems [9] and can be explained as the consequence of the pairing of particles, that reduces the effective aspect ratio of the cluster of associated particles, destabilizing the nematic phase.

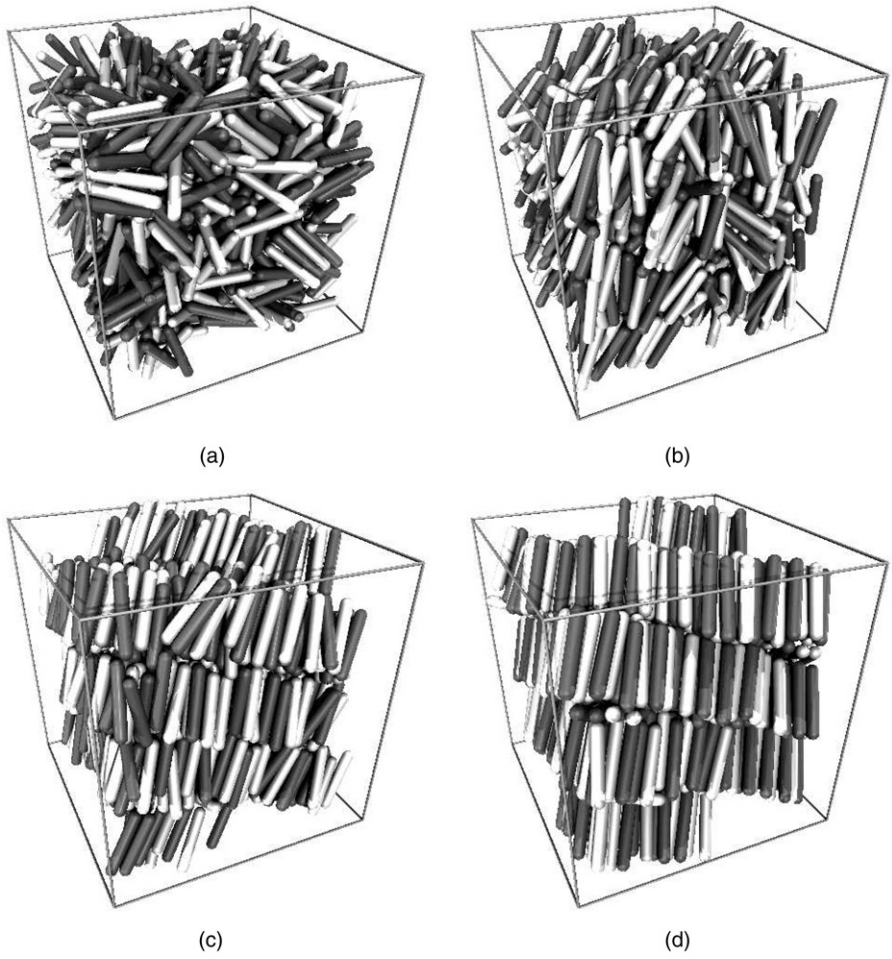

Figure 2. Snapshots for different configurations for a system of 1020 CHSC of aspect ratio $L/\sigma = 5$ at temperature $T = 0.2$ obtained by NPT-MC simulations. The configurations correspond to (a) the highest-density isotropic state ($P^* = 5.00$), (b) the nematic state ($P^* = 5.25$), (c) the lowest-density smectic-A state ($P^* = 5.50$), and (d) the highest-density smectic-A phase ($P^* = 10.40$).

To fully define the N–SmA phase transition, the nematic order parameter, S and the orientational correlation function are not enough, and additional statistical functions are required to characterize the longitudinal layer's correlations, typical of smectic phases. Two standard choices can be used: the smectic order parameter, τ, which is the first order Fourier representation of the density along the direction of the layers [33–35], and the projection of the pair correlation function along the director, $g_{||}(r_{||})$. In this work, the latter has been chosen and is given in Figure 5, where we can see a clear formation of modulated peaks produced by the layering of the system at high densities in the smectic phases. The separation between neighbour peaks is proportional to the layering spacing, which is slightly higher than about 6σ, i.e. slightly higher than the total length of the particles. Pre-transition layering in the N state can also be observed in Figure 5. In order to characterize the smectic phases, we have analysed the behaviour of the projection of the pair correlation function perpendicular to the director, $g_{\perp}(r_{\perp})$. This is shown in Figure 6, which clearly indicates the presence of a SmA phase since the correlation decays, with a lack of long-range order for values of the pressure up to $P^* = 10.40$. Analysing the overall behaviour of the data presented in Figure 1, it can be observed that reducing the temperature tends to increase the range of stabilization of the SmA phase. This behaviour is enhanced for the ion-pairing of the central charges, increasing the alignment of the particles in layers. The same stabilization of the smectic phase was observed for HSC with central longitudinal dipoles [9].

The ion-pairing effect in the smectic phases is interesting and requires further attention. Smectic layers behave as quasi-2D systems, where different

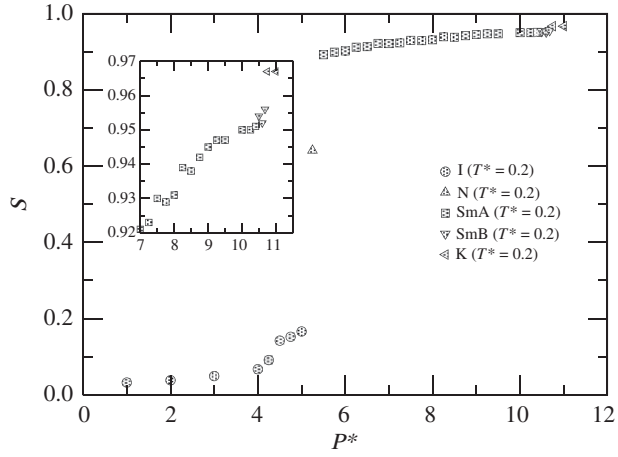

Figure 3. Nematic order parameter, S, as a function of the pressure, P^*, for a system of 1020 CHSC of aspect ratio $L/\sigma = 5$ at temperature $T^* = 0.2$ obtained by NPT-MC simulations.

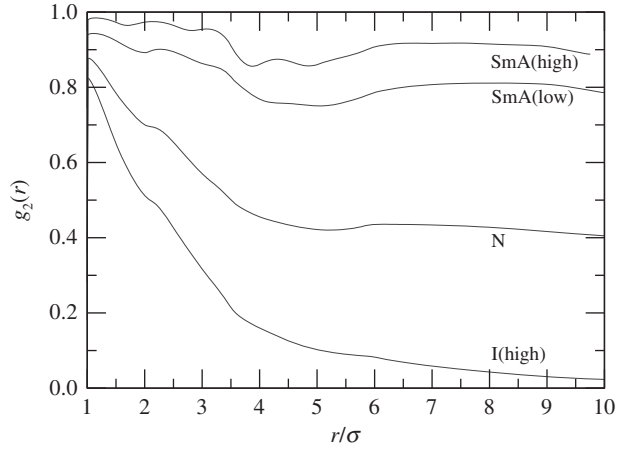

Figure 4. The orientational correlation function, $g_2(r)$, for a system of 1020 CHSC of aspect ratio $L/\sigma = 5$ at temperature $T^* = 0.2$ obtained by NPT-MC simulations. The data depicted are for the highest-density isotropic state ($P^* = 5.00$), the nematic state ($P^* = 5.25$), the lowest-density smectic-A state ($P^* = 5.50$), and the highest-density smectic-A phase ($P^* = 10.40$).

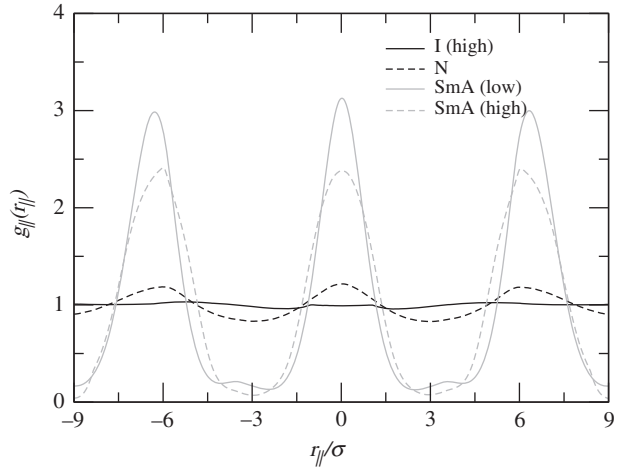

Figure 5. Projection of the radial distribution function parallel to the director, $g_{||}(r_{||})$, for a system of 1020 CHSC of aspect ratio $L/\sigma = 5$ at temperature $T^* = 0.2$ obtained by NPT-MC simulations. The data depicted are for the highest-density isotropic state ($P^* = 5.00$), the nematic state ($P^* = 5.25$), the lowest-density smectic-A state ($P^* = 5.50$), and the highest-density smectic-A phase ($P^* = 10.40$).

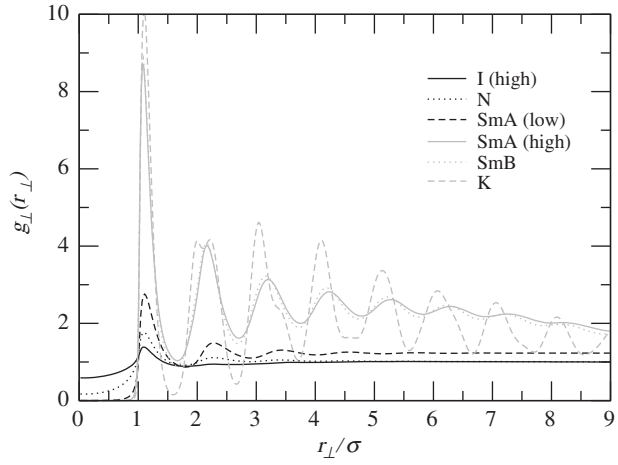

Figure 6. Projection of the radial distribution function perpendicular to the director, $g_{\perp}(r_{\perp})$, for a system of 1020 CHSC of aspect ratio $L/\sigma = 5$ at temperature $T^* = 0.2$ obtained by NPT-MC simulations. The data depicted are for the highest-density isotropic state ($P^* = 5.00$), the nematic state ($P^* = 5.25$), the lowest-density smectic-A state ($P^* = 5.50$), the highest-density smectic-A phase ($P^* = 10.40$), the hexatic phase ($P^* = 10.60$), and the lowest-density crystal state ($P^* = 10.75$).

structured patterns appear. It is possible to observe a transition between disorder and quasi-long range order, characterized by a power-law decay of the sixfold orientational correlations [31,36,37], signalling the presence of an hexatic ordering, i.e. the possible formation of a smectic-B (SmB) phase. This hexatic phase appears as an intermediate phase between a disordered-liquid and an hexagonal crystalline phase, and has been observed in experiments in thermotropic LC systems [38–41], LC films [41–43], colloidal LC systems [44,45], and chiral rod-like viruses [46], to give some examples. In molecular simulation the hexatic behaviour in smectic phases has also been observed in parallel soft spherocylinders [47,48], in a bead necklace model [49], and in Gay–Berne particles [50–54]. However, the last system is still a matter of debate [55]. Since metastable hexatic phases can be observed in strict 2D systems [32], a proper size-effects study is required to be implemented in order to

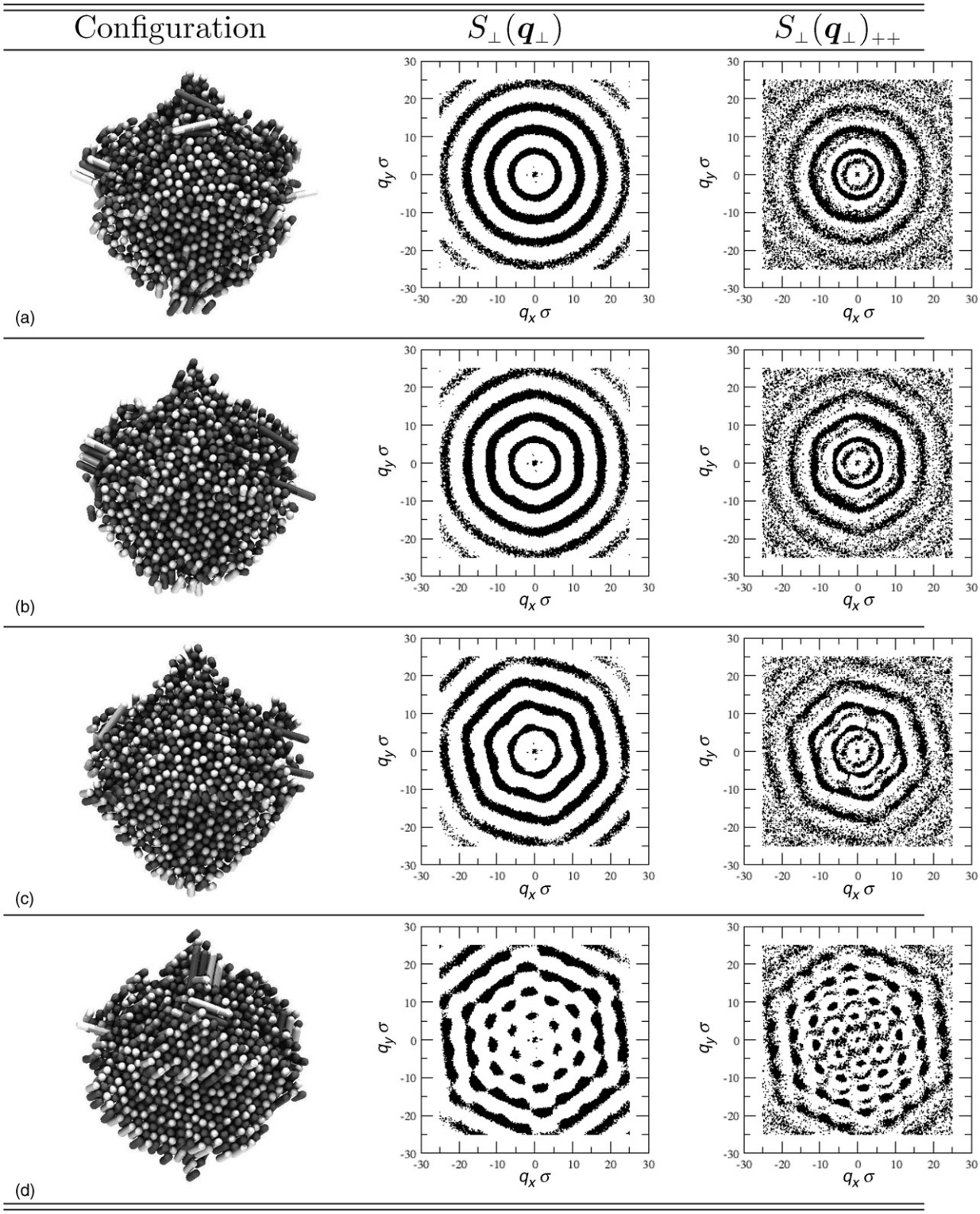

Figure 7. Snapshots for different high-density layered states, and the projections of the total, $S_\perp(\boldsymbol{q}_\perp)$, and charge–charge, $S_\perp(\mathbf{q}_\perp)_{++}$, structure factors at temperature $T^* = 0.2$. The figures correspond to (a) the highest-density smectic-A state ($P^* = 10.40$), (b) the lowest-density hexatic state ($P^* = 10.50$), (c) the highest-density hexatic state ($P^* = 10.68$), and (d) the lowest-density crystal state ($P^* = 10.75$).

Table 2. Hexagonal bond-orientational order parameter, Ψ_6, calculated for the CHSC system in layered phases, as a function of the reduced pressure, P^*, at temperatures $T^* = 0.2$ and $T^* = 0.5$.

P^*	Ψ_6 ($T^* = 0.2$)	Ψ_6 ($T^* = 0.5$)
6.75	0.032 ± 0.017	0.029 ± 0.015
7.50	0.034 ± 0.018	0.034 ± 0.018
8.25	0.036 ± 0.017	0.037 ± 0.022
9.00	0.046 ± 0.025	0.042 ± 0.023
9.50	0.050 ± 0.025	0.055 ± 0.028
10.00	0.076 ± 0.032	0.065 ± 0.035
10.40	0.073 ± 0.034	0.110 ± 0.050
10.50	0.136 ± 0.069	0.086 ± 0.037
10.60	0.187 ± 0.060	0.745 ± 0.020
10.68	0.285 ± 0.050	0.766 ± 0.015
10.75	0.643 ± 0.026	0.765 ± 0.016
11.00	0.705 ± 0.021	0.773 ± 0.015

determine the stability of the SmB phase observed for the CHSC system studied here.

We have analysed the behaviour of the smectic phases in CHSC for further compression of the system at the same isotherm of $T^* = 0.2$ to investigate whether or not this system presents hexatic ordering. For this purpose, we have calculated the projection of the structure factor $S_\perp(\boldsymbol{q}_\perp)$ in the planes of the layers, which is close to the scattering experiments in real systems, and by calculating the hexagonal bond orientational order-parameter, Ψ_6. The projections of the structure factor, $S_\perp(\boldsymbol{q}_\perp)$, the related $S_{\perp,++}(\boldsymbol{q}_{\perp,++})$, and the snapshots for selected layers for different smectic and crystalline phases are shown in Figure 7. In Table 2 and in Figure 8, we present the values for the hexagonal bond-orientational order parameter as a function of the pressure. At high pressure ($P^* \geq 10.75$) the system tends to form as a crystalline (K) structure, where the well-defined Bragg's peaks typical of hexagonal order can be observed. The crystalline structure is also given by $g_\perp(r_\perp)$ (see Figure 6), where the long range positional order of the particles in the layers is evident. For pressures in the range $10.50 \leq P^* \leq 10.68$, we have observed that the hexagonal Bragg's peaks disappear, but the hexagonal-like order is still present. This is typical behaviour of hexatic ordering, where the long-range translational order is lost, but the long-range orientational order remains. However, it's very well known that in 2D the effect of the fluctuations are enhanced compared to the 3D case, and further finite-size effects analysis will be needed in order to confirm that the system is not in a metastable region [32]. As can be seen in Table 2, for the isotherm of $T^* = 0.5$ the hexatic ordering was not observed.

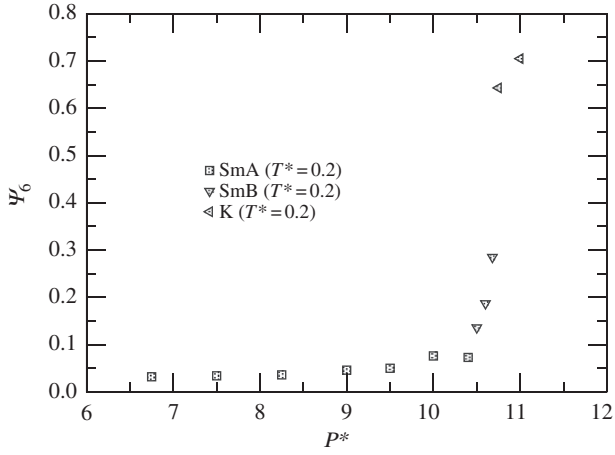

Figure 8. Hexagonal bond-orientational order parameter, Ψ_6 as a function of the pressure, P^*, for a system of 1020 CHSC of aspect ratio $L/\sigma = 5$ at temperature $T^* = 0.2$ obtained by NPT-MC simulations.

4. Conclusions

In this work we have presented the study at low temperatures for CHSC of aspect ratio $L/\sigma = 5$ using NPT-MC simulations. As observed in our previous work, coulombic forces enhance the range of stability of both the I and SmA phases, in a similar way as observed for HSC with central longitudinal dipoles [9] and CHSC at temperatures $T^* \geq 0.5$ [7]. It has also been observed that the range of stability of the N phase is reduced considerably, which indicates the presence of a triple point at lower temperatures. A further free energy analysis for this issue is required in order to trace the phase diagram, using, for example, the Gibbs–Duhem technique [5,56–58]. The same destabilization of the N phase was also observed in dipolar HSC, where the effect of dipole pairing decreases the aspect ratio of the cluster of associating particles, bearing in mind that for short HSC ($L/\sigma \leq 3.2$) the N phase is not observed. At high pressure, between the SmA and K phases, we have detected the formation of a smectic phase with hexatic order (SmB phase) in the planes of the layers. This effect has been detected analysing the projection of the structure factor in these planes, where the Bragg's peaks in the K phases tend to disappear (loss of translational order), and the hexagonal-like order still remains. However, a further analysis is required in order to determine the stability of this phase, since the system used in this study is not large enough to give a definitive conclusion. Finally, another effect that deserves to be studied in detail is the role that could be played by the flexibility

of liquid crystal molecules on the stability of the phases, as previously reported by several authors [12,59–61]. Flexible tails in hard rod-like particles tend to enhance the stability of smectic and crystalline phases, suppressing the nematic phase [12]. However, the addition of a terminal dipole at the end cap (opposite the flexible tail) does not suppress any of the LC phases observed in HSC. Primitive models of flexible LC systems could be investigated using CHSC molecules with flexible tails as an initial representation, to compare with real rod-like ionic liquid crystals.

Acknowledgements

Financial support for this work was given by PROMEP (México), and Consejo Nacional de Ciencia y Tecnología (CONACYT, México), through a PhD scholarship (G.J.S.) and grants 61418, 58470. C.A. also acknowledges the United Kingdom Engineering and Physical Sciences Research Council (EPSRC) Grant No. EP/E016340, 'Molecular System Engineering'.

References

[1] M.P. Allen, G.T. Evans, D. Frenkel and B.M. Mulder, Adv. Chem. Phys. **86**, 1 (1993).
[2] L. Onsager, Ann. N.Y. Acad. Sci. **51**, 627 (1949).
[3] D. Frenkel, J. Phys. Chem. **92**, 3280 (1988).
[4] S.C. McGrother, D.C. Williamson and G. Jackson, J. Chem. Phys. **104**, 6755 (1996).
[5] P. Bolhuis and D. Frenkel, J. Chem. Phys. **106**, 666 (1997).
[6] P.T. Collings and M. Hird, *Introduction to Liquid Crystals* (Taylor & Francis, London, 1997).
[7] C. Avendaño, A. Gil-Villegas and E. González-Tovar, J. Chem. Phys. **128**, 044506 (2008).
[8] A. Gil-Villegas, S.C. McGrother and G. Jackson, Mol. Phys. **92**, 723 (1997).
[9] S.C. McGrother, A. Gil-Villegas and G. Jackson, Mol. Phys. **95**, 657 (1998).
[10] A. Gil-Villegas, G. Jackson and S.C. McGrother, J. Mol. Liq. **76**, 171 (1998).
[11] S.C. McGrother, A. Gil-Villegas and G. Jackson, J. Phys. Condes. Matter **8**, 9649 (1996).
[12] J.S. van Duijneveldt, A. Gil-Villegas, G. Jackson and M.P. Allen, J. Chem. Phys. **112**, 9092 (2000).
[13] A. Gil-Villegas, S.C. McGrother and G. Jackson, Chem. Phys. Lett. **269**, 441 (1997).
[14] C. Avendaño, A. Gil-Villegas and E. González-Tovar, Chem. Phys. Lett. **470**, 67 (2009).
[15] M.P. Allen and D.J. Tildesley, *Computer Simulation of Liquids* (Oxford University Press, Oxford, 1987).
[16] D. Frenkel and B. Smit, *Understanding Molecular Simulation* , 2nd ed (Academic Press, London, 2002).
[17] C. Avendaño and A. Gil-Villegas, Mol. Phys. **104**, 1475 (2006).
[18] C. Avendaño, N. Ibarra-Avalos, C.M. Quezada, J. Medina and A. Gil-Villegas, Rev. Mex. Fís. **52**, 85 (2006).
[19] D. Wolf, Phys. Rev. Lett. **68**, 3315 (1992).
[20] D. Wolf, P. Keblinski, S.R. Phillpot and J. Eggebrecht, J. Chem. Phys. **110**, 8254 (1999).
[21] P. Demontis, S. Spanu and G.B. Suffritti, J. Chem. Phys. **114**, 7980 (2001).
[22] D. Zahn, B. Schilling and S. Kast, J. Phys. Chem. B **106**, 10725 (2002).
[23] C.J. Fennell and J.D. Gezelter, J. Chem. Phys. **124**, 234104 (2006).
[24] T.S. Mahadevan and S.H. Garofalini, J. Phys. Chem. B **111**, 8919 (2007).
[25] F.N. Mendoza, J. Lopez-Lemus, G.A. Chapela and J. Alejandre, J. Chem. Phys. **129**, 024706 (2008).
[26] S.W. De Leeuw, J.W. Perram and E.R. Smith, Proc. R. Soc. A **373**, 27 (1980).
[27] M. Deserno and C. Holm, J. Chem. Phys. **109**, 7678 (1998).
[28] M. Deserno and C. Holm, J. Chem. Phys. **109**, 7694 (1998).
[29] R.J. Low, Eur. J. Phys. **23**, 111 (2002).
[30] J.A.C. Veerman and D. Frenkel, Phys. Rev. A **41**, 3237 (1990).
[31] P.M. Chaikin and T.C. Lubensky, *Principles of Condensed Matter Physics* (Cambridge University Press, England, 1995).
[32] S.J. Mejía-Rosales, A. Gil-Villegas, B.I. Ivlev and J. Ruiz-García, J. Phys. Chem. B **110**, 22230 (2006).
[33] S. Singh, Phys. Rep. **324**, 107 (2000).
[34] R.E. Webster, N.J. Mottram and D.J. Cleaver, Phys. Rev. E **68**, 021706 (2003).
[35] C. Avendaño and E.A. Müller, Phys. Rev. E **80**, 061702 (2009).
[36] J.M. Kosterlitz and D.J. Thouless, J. Phys. C **6**, 1181 (1973).
[37] B.I. Halperin and D.R. Nelson, Phys. Rev. Lett. **41**, 121 (1978).
[38] D.E. Moncton and R. Pindak, Phys. Rev. Lett. **43**, 701 (1979).
[39] A.J. Leadbetter, M.A. Mazid, B.A. Kelly, J.W. Goodby and G.W. Gray, Phys. Rev. Lett. **43**, 630 (1979).
[40] R. Pindak, D.E. Moncton, S.C. Davey and J.W. Goodby, Phys. Rev. Lett. **46**, 1135 (1981).
[41] R. Geer, T. Stoebe, C.C. Huang, R. Pindak, J.W. Goodby, M. Cheng, J.T. Ho and S.W. Hui, Nature **355**, 152 (1992).
[42] M. Cheng, J.T. Ho, S.W. Hui and R. Pindak, Phys. Rev. Lett. **59**, 1112 (1987).
[43] M. Cheng, J.T. Ho, S.W. Hui and R. Pindak, Phys. Rev. Lett. **61**, 550 (1988).
[44] A.V. Petukhov, D. van der Beek, R.P.A. Dullens, I.P. Dolbnya, G.J. Vroege and H.N.W. Lekkerkerker, Phys. Rev. Lett. **95**, 077801 (2005).
[45] B.J. Lin and L.J. Chen, J. Chem. Phys. **126**, 034706 (2007).

[46] E. Grelet, Phys. Rev. Lett. **100**, 168301 (2008).
[47] K.M. Aoki and F. Yonezawa, Phys. Rev. Lett. **69**, 2780 (1992).
[48] K.M. Aoki, M. Yoneya and H. Yokoyama, Phys. Rev. E **81**, 021701 (2010).
[49] L. De Gaetani and A. Tani, J. Chem. Phys. **126**, 064909 (2007).
[50] L.F. Rull, Physica A **220**, 113 (1995).
[51] J.T. Brown, M.P. Allen, E. Martín del Río and E. de Miguel, Phys. Rev. E **57**, 6685 (1998).
[52] M.A. Bates and G.R. Luckhurst, J. Chem. Phys. **110**, 7087 (1999).
[53] E. de Miguel, E.M. del Rio and F.J. Blas, J. Chem. Phys. **121**, 11183 (2004).
[54] M. Houssa, L.F. Rull and J.M. Romero-Enrique, J. Chem. Phys. **130**, 154504 (2009).
[55] E. de Miguel and C. Vega, J. Chem. Phys. **117**, 6313 (2002).
[56] D.A. Kofke, J. Chem. Phys. **98**, 4149 (1993).
[57] D.A. Kofke, Mol. Phys. **78**, 1331 (1993).
[58] C. Vega, E. Sanz, J.L.F. Abascal and E.G. Noya, J. Phys. Condes. Matter **20**, 153101 (2008).
[59] J.S. van Duijneveldt and M.P. Allen, Mol. Phys. **92**, 855 (1997).
[60] H. Fynewever and A. Yethiraj, J. Chem. Phys. **108**, 1636 (1998).
[61] C. McBride and C. Vega, J. Chem. Phys. **117**, 10370 (2002).